

Neutral delay differential equation Kerr cavity model

Andrei G. Vladimirov, Daria A. Dolinina

submitted: June 27, 2023

Weierstrass Institute
Mohrenstr. 39
10117 Berlin
Germany
E-Mail: andrei.vladimirov@wias-berlin.de
daria.dolinina@wias-berlin.de

No. 3025
Berlin 2023



2020 Mathematics Subject Classification. 78A60, 34K40.

2010 Physics and Astronomy Classification Scheme. 42.65.-k, 42.65.Sf, 42.65.Pc, 42.65.Tg.

Key words and phrases. Temporal cavity solitons, neutral delay differential equation model, passive optical cavity.

Stimulating discussions with Guillaume Huyet, Dmitry Turaev, and Matthias Wolfrum, as well as the support by the Deutsche Forschungsgemeinschaft (DFG projects No. 445430311 and No. 491234846) are gratefully acknowledged.

Edited by
Weierstraß-Institut für Angewandte Analysis und Stochastik (WIAS)
Leibniz-Institut im Forschungsverbund Berlin e. V.
Mohrenstraße 39
10117 Berlin
Germany

Fax: +49 30 20372-303
E-Mail: preprint@wias-berlin.de
World Wide Web: <http://www.wias-berlin.de/>

Neutral delay differential equation Kerr cavity model

Andrei G. Vladimirov, Daria A. Dolinina

Abstract

A neutral delay differential equation (NDDE) model of a Kerr cavity with external coherent injection is developed that can be considered as a generalization of the Ikeda map with second and higher order dispersions being taken into account. It is shown that this model has solutions in the form of dissipative solitons both in the limit, where the model can be reduced to the Lugiato-Lefever equation (LLE), and beyond this limit, where the soliton is eventually destroyed by the Cherenkov radiation. Unlike the standard LLE the NDDE model is able to describe the overlap of multiple resonances associated with different cavity modes.

1 Introduction

Over the last two decades, optical frequency combs have found applications in different fields of science and industry including spectroscopy, optical ranging, metrology, searching for exoplanets, microwave photonics and optical communications [5, 27, 25, 29, 30, 38]. Standard methods of the frequency comb generation are based on the use of mode-locked lasers [17] and optical microcavities subject to an external coherent injection [6]. One of the most commonly used methods to model Kerr optical cavities is based on the application of the paradigmatic Lugiato-Lefever equation (LLE) [23], which is known to exhibit bistability of continuous wave (CW) solutions as well as dissipative soliton solutions preserving their shape in the course of propagation along the cavity axis and sitting on a constant intensity background. The latter solutions correspond to the so-called temporal cavity solitons (TCSs), which were observed experimentally in optical microresonator frequency comb generators [14], optical fiber cavities [22], and mode-locked lasers [10]. The LLE based on the mean-field approximation is, however, not free from certain shortcomings. In particular, it describes bistable behavior and TCS formation only in the vicinity of a single cavity resonance [2, 14]. To overcome this shortcoming the modeling approaches based on the so-called generalized Ikeda map [24, 12, 3, 4, 13] and a generalized LLE model with localized injection and losses [20] were developed to describe the appearance of the overlap of multiple nonlinear resonances, multistability of CW solutions, and super-solitons [13]. Here we propose an alternative approach to model nonlinear dynamics of an injected Kerr cavity based on second order neutral type delay differential equation (NDDE), which also can be considered as a generalization of the Ikeda map [16]. We show that in a certain limit the NDDE model can be reduced to the LLE. We perform linear stability analysis of the NDDE model in the practically important large delay limit and present numerical evidence of the existence of stationary and oscillating dissipative optical solitons in it. We show that beyond the LLE limit the TCSs of the NDDE model are strongly affected by the Cherenkov radiation induced by the high order dispersion. The modeling approach proposed here can be adopted to study the dynamics of solid state and fiber lasers, where the chromatic dispersion of the intracavity media plays an important role in the mechanism of the short pulse generation as well as to investigate the effect of second and higher order dispersion on the characteristics of mode-locking regimes in semiconductor lasers. Furthermore, the NDDE model

might be useful to model the coupled-cavity systems such as microcavity optical frequency comb generator pumped by a semiconductor mode-locked light source, which is already successfully modeled by DDE models [33, 34, 32, 31].

2 Model equation

A neutral delay differential equation (NDDE) model of a ring Kerr cavity subject to a coherent optical injection reads:

$$\begin{aligned} \left(A + a\partial_t A + \frac{a^2 - ib}{2}\partial_{tt} A \right) e^{-i\alpha|A|^2/2 - i\theta/2} \\ = \sqrt{\kappa} \left(A_\tau - a\partial_t A_\tau + \frac{a^2 + ib}{2}\partial_{tt} A_\tau \right) e^{i\alpha|A_\tau|^2/2 + i\theta/2} + \eta, \end{aligned} \quad (1)$$

where t is the time, $A(t)$ is the normalized electric field envelope, $A_\tau = A(t - \tau)$ is the retarded field amplitude with the delay time τ equal to the linear round-trip time of the cavity. α is the Kerr coefficient, κ is the linear intensity attenuation factor per cavity round-trip, η is the normalized injection rate, and θ describes the detuning between the injection frequency and the frequency of a cavity mode. The coefficients $a > 0$ and b are responsible for the intracavity dispersion. Note, that, as it will be shown below, in the LLE limit only the coefficient b contributes to the second order dispersion, while the parameter a describes the group delay due to the first order dispersion. In the absence of injection and losses, $\eta = 0$ and $\kappa = 1$, Eq. (1) is similar to the conservative version of the Gires–Tournois interferometer model introduced in [28]. Similarly to this model Eq. (1) with $\eta = 0$ and $\kappa = 1$ is symmetric under the transformation $t \rightarrow -t$ and $A \rightarrow A^*$ combined with the time shift and, hence, it is reversible in the non-dissipative limit. Note, however, that unlike the first order NDDE Gires–Tournois interferometer model studied in [28] the second order derivative terms responsible for the second order dispersion in the LLE limit are present in Eq. (1), see also Ref. [26]. This is an important difference between Eq. (1) and the model of Ref. [28]. Note, that for $a = b = 0$ Eq. (1) becomes similar to the well known Ikeda map [16]. The derivation of Eq. (1) is given in the next section together with the derivation of three other versions of the NDDE model including the mean field one. An advantage of the model equation (1) is that in the non-dissipative limit, $\eta = 0$ and $\kappa = 1$, similarly to the first order NDDE discussed in [28] it admits a relatively simple conserved quantity $\partial_t W(t) = 0$ with

$$\begin{aligned} W(t) = a^3 |\partial_t A(t)|^2 + ib [A(t) \partial_t A^*(t) - A^*(t) \partial_t A(t)] + 2a |A(t)|^2 \\ + \int_t^{t+\tau} \left| A(x) + a\partial_x A(x) + \frac{a^2 - ib}{2}\partial_{xx} A(x) \right|^2 dx. \end{aligned}$$

Therefore this study is mainly focused on the analysis of Eq. (1).

3 Model derivation

To derive the NDDE model let us consider the schematic representation of a ring Kerr cavity with a pair of thin dispersive (phase) filters and two identical Kerr media shown in Fig. 1. The field envelope on the output of the left Kerr medium is given by $A_2(t + \tau_1) = A_1(t) e^{i\alpha|A_1(t)|^2/2 + i\phi_1}$, where α is the

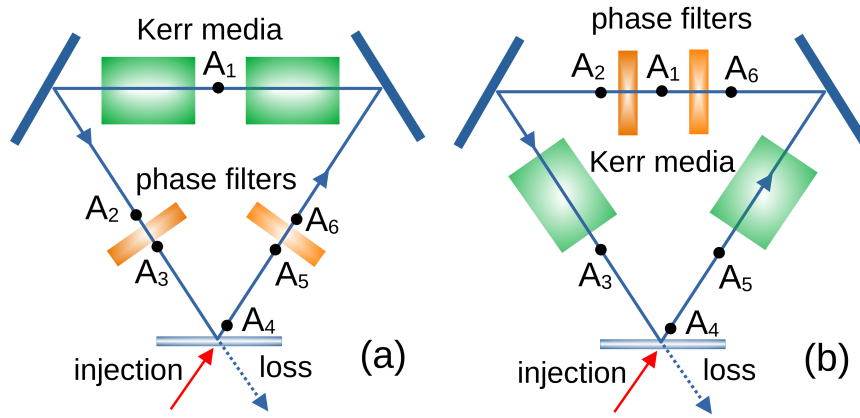


Figure 1: Ring cavity with two Kerr media (green) and a pair of identical thin phase filters (orange) responsible for the intracavity dispersion.

Kerr coefficient, ϕ_1 and τ_1 are the phase shift and the delay time due to the propagation in the cavity, see Fig. 1(a).

The Fourier transform of the field envelope at the output from a phase filter is given by $\hat{A}_3(\omega) = \hat{f}(\omega) \hat{A}_2(\omega)$, where $\hat{A}_2(\omega)$ is the Fourier transform of the input field $A_2(t)$ and $\hat{f}(\omega) = e^{-i\Phi(\omega)}$ with real $\Phi(\omega)$, see e. g. Ref. [15]. Close to $\omega = 0$ we can use the expansion

$$\hat{f}(\omega) = e^{-i\Phi(0)} \left\{ 1 + i\omega\Phi'(0) - [\Phi'(0)^2 - i\Phi''(0)]\omega^2/2 + \mathcal{O}(\omega^3) \right\}.$$

Taking this relation into account, the electric field envelope A_3 can be expressed as

$$\begin{aligned} A_3(t) &= \mathcal{F}^{-1} \left[\hat{f}(\omega) \hat{A}_2(\omega) \right] = \mathcal{F}^{-1} \left\{ e^{-i\phi/2} \left[1 + i\omega a - \frac{a^2 + ib}{2}\omega^2 + \mathcal{O}(\omega^3) \right] \hat{A}_2(\omega) \right\} \\ &= \left[1 - a\partial_t + \frac{a^2 + ib}{2}\partial_{tt} + \mathcal{O}(\partial_{ttt}) \right] A_2(t) e^{-i\phi/2}, \end{aligned} \quad (2)$$

where \mathcal{F}^{-1} is the inverse Fourier transform and the notations $\Phi(0) \equiv \phi$, $\Phi'(0) \equiv a$, and $\Phi''(0) \equiv -b$ are used. The field amplitude A_4 is obtained from A_3 by taking into account time delay τ_2 , phase shift ϕ_2 , and introducing the injection rate η , and the intensity attenuation factor κ due to the cavity losses. Thus we get

$$A_4\left(t + \frac{\tau}{2}\right) = \sqrt{\kappa} \left[1 - a\partial_t + \frac{a^2 + ib}{2}\partial_{tt} + \mathcal{O}(\partial_{ttt}) \right] \left(A_1 e^{i\alpha|A_1|^2/2 + i\theta/2} \right) + \eta, \quad (3)$$

with the one half of the cavity round trip time $\tau/2 = \tau_1 + \tau_2$ and the phase shift $\theta/2 = -(\phi_1 + \phi + \phi_2)$.

The field envelope on the input of the left Kerr medium is given by $A_6(t - \tau_1) = A_1(t) e^{-i\alpha|A_1(t)|^2/2 - i\phi_1}$ with $|A_1(t)|^2 = |A_6(t - \tau_1)|^2$. The Fourier transform of the field envelope A_6 is given by $\hat{A}_6(t) = \hat{f}(\omega) \hat{A}_5(\omega)$, which can be rewritten as $\hat{A}_5(t) = \hat{f}^{-1}(\omega) \hat{A}_6(\omega) = \hat{f}^*(\omega) \hat{A}_6(\omega)$. Hence we get

$$A_5(t) = \mathcal{F}^{-1} \left[\hat{f}^*(\omega) \hat{A}_6(\omega) \right] = \left[1 + a\partial_t + \frac{a^2 - ib}{2}\partial_{tt} + \mathcal{O}(\partial_{ttt}) \right] A_6(t) e^{-i\phi/2}.$$

Therefore, similarly to (3) we obtain

$$A_4\left(t - \frac{\tau}{2}\right) = \left[1 + a\partial_t + \frac{a^2 - ib}{2}\partial_{tt} + \mathcal{O}(\partial_{ttt}) \right] \left(A_1 e^{-i\alpha|A_1|^2/2 - i\theta/2} \right). \quad (4)$$

Finally, shifting the time in Eq. (3) by $-\tau$, equating the resulting equation to Eq. (4), and neglecting high order dispersion terms $\mathcal{O}(\partial_{ttt})$ we get

$$\begin{aligned} & \left(1 + a\partial_t + \frac{a^2 - ib}{2}\partial_{tt}\right) \left(Ae^{-i\alpha|A|^2/2 - i\theta/2}\right) \\ & = \sqrt{\kappa} \left(1 - a\partial_t + \frac{a^2 + ib}{2}\partial_{tt}\right) \left(A_\tau e^{i\alpha|A_\tau|^2/2 + i\theta/2}\right) + \eta, \end{aligned} \quad (5)$$

where $A \equiv A_1$ and $A_\tau = A(t - \tau)$.

The model (1) can be derived in a similar way to Eq. (5), see Fig. 1(b). Here neglecting the high order dispersions we get:

$$A_2 \approx A_1 - a\partial_t A_1 + \frac{a^2 + ib}{2}\partial_{tt} A_1, \quad (6)$$

and

$$A_4 \left(t + \frac{\tau}{2}\right) \approx \sqrt{\kappa} A_2 e^{i\alpha|A_2|^2/2 + i\theta/2} + \eta. \quad (7)$$

Substituting Eq. (6) into Eq. (7), assuming that a , b , and α are sufficiently small, and neglecting the $\mathcal{O}(\alpha a)$ and $\mathcal{O}(\alpha b)$ terms in the exponential we obtain

$$A_4 \left(t + \frac{\tau}{2}\right) \approx \sqrt{\kappa} \left(A_1 - a\partial_t A_1 + \frac{a^2 + ib}{2}\partial_{tt} A_1\right) e^{i\alpha|A_1|^2/2 + i\theta/2} + \eta. \quad (8)$$

Similarly, for another half of the cavity, we get

$$A_4 \left(t - \frac{\tau}{2}\right) \approx \left(A_1 + a\partial_t A_1 + \frac{a^2 - ib}{2}\partial_{tt} A_1\right) e^{-i\alpha|A_1|^2/2 - i\theta/2}. \quad (9)$$

Finally, combining Eqs. (8) and (9) we arrive at the NDDE model (1). The latter equation can be further simplified under the approximation $\alpha a, \alpha b \ll 1$, which was already used above:

$$\begin{aligned} & \left(Ae^{-i\alpha|A|^2/2} + a\partial_t A + \frac{a^2 - ib}{2}\partial_{tt} A\right) e^{-i\theta/2} \\ & = \sqrt{\kappa} \left(A_\tau e^{i\alpha|A|^2/2} - a\partial_t A_\tau + \frac{a^2 + ib}{2}\partial_{tt} A_\tau\right) e^{i\theta/2} + \eta, \end{aligned} \quad (10)$$

In the mean field approximation, where the field amplitude is small, expanding the exponentials in Eq. (10) we get the following equation:

$$\begin{aligned} & \left(A + a\partial_t A + \frac{a^2 - ib}{2}\partial_{tt} A - i\frac{\alpha}{2}|A|^2\right) e^{-i\theta/2} \\ & = \sqrt{\kappa} \left(A_\tau - a\partial_t A_\tau + \frac{a^2 + ib}{2}\partial_{tt} A_\tau + i\frac{\alpha}{2}|A_\tau|^2\right) e^{i\theta/2} + \eta. \end{aligned} \quad (11)$$

Neutral DDEs (1), (5), (10), and (11) are reversible in the non-dissipative limit $\eta = 0$ and $\kappa = 1$. This property is similar to that of the LLE, which will be derived from these equations in the next section. As it will be shown in the next section, the parameter b corresponds to the second order dispersion coefficient in the LLE limit. In the absence of dispersion according to Eq. (6) the field amplitude on the output of the phase filter is defined by

$$A_2 \approx A_1 - a\partial_t A_1 + \frac{a^2}{2}\partial_{tt} A_1 = A_1(t - a) + \mathcal{O}(a^3).$$

Therefore, the parameter a has the meaning of the group delay introduced by the filter. The inequality $a > 0$ follows from the causality principle. As it will be shown below this inequality is the necessary but not sufficient condition of the absence of a spurious instability in the NDDE models.

Note, that a straightforward derivation of the model equation without splitting Kerr and dispersive media into two symmetric parts would result in a “regular” DDE model instead of NDDE:

$$A + 2a\partial_t A + (a^2 - ib) \partial_{tt} A = \sqrt{\kappa} A (t - \tau) e^{i\alpha|A(t-\tau)|^2 + i\theta} + \eta, \quad (12)$$

which is a generalization of the Ikeda map and is very similar to the model derived in [26] to describe a Kerr cavity with two spectral filters. However, unlike the NDDE model (1) having no spectral filtering, the LLE obtained from Eq. (12) contains an additional large diffusion term proportional to a^2 [26] in addition to the second order dispersion term proportional to b . Therefore, this model is not suitable to describe a multimode Kerr cavity characterized by a strong dispersion in combination with small spectral filtering.

To conclude this section, we note that the derivation presented here can be trivially generalized by including higher order dispersion terms into the model equation.

4 Reduction to the LLE

Using the multiscale method described in [21] we can derive the same LLE from any one of the four model equations (1), (5), (10), and (11). To be more specific, we choose Eq. (1) and in the large delay limit $\tau = \epsilon^{-1} \gg 1$ rescale the time as $x = \epsilon t$ to get

$$\begin{aligned} & \left(A + \epsilon a \partial_x A + \epsilon^2 \frac{a^2 - ib}{2} \partial_{xx} A \right) e^{i\alpha|A|^2/2 + i\theta/2} = \\ & \sqrt{\kappa} \left(A_{\tau_1} - \epsilon a \partial_x A_{\tau_1} + \epsilon^2 \frac{a^2 + ib}{2} \partial_{xx} A_{\tau_1} \right) e^{i\alpha|A_{\tau_1}|^2/2 + i\theta/2} + \eta, \end{aligned} \quad (13)$$

where $A_{\tau_1} = A(t - 1)$. Next, we introduce two time scales $A(t) = u(t_0, t_2)$, where $t_0 = (1 - \epsilon c_1 + \epsilon^2 c_2 + \dots)x$, $t_2 = \epsilon^2 x$, and rescale the parameters as

$$\alpha = \epsilon^2 \chi, \quad \kappa = e^{-2\epsilon^2 k}, \quad \eta = \epsilon^2 r. \quad (14)$$

Substituting these expressions into Eq. (13), collecting the first order terms in ϵ , and using the Fredholm alternative we obtain the following boundary condition

$$u(t_0, t_2) = u(t_0 - 1, t_2) e^{i\theta}, \quad (15)$$

together with the relation $c_1 = 2a$ for the group delay parameter. Finally, collecting the second order terms in ϵ we get $c_2 = 4a^2$ and the LLE model:

$$\partial_{t_2} u = -ku + i\chi u |u|^2 + ib \partial_{t_0 t_0} u + r. \quad (16)$$

Note that Eq. (16) with the boundary condition (15), where the parameter θ plays the role of the detuning, is able to describe multiple resonances corresponding to different cavity modes. However, it cannot describe the overlap of these resonances. In order to get overlapping resonances and coexisting different solitons one needs to replace distributed injection and losses with the localized ones, as it was proposed in [20]. It is seen from Eq. (16) that the coefficient b in front of the second derivative

terms is responsible for the second order dispersion in the LLE limit, see also [26]. Therefore, these derivatives cannot be neglected in the model equation. Away from the LLE limit coefficient a might also contribute to the second order dispersion, which, in particular, can follow from the numerical results of [28], where a first order NDDE was studied.

Using the additional assumption that the detuning is small,

$$\theta = -\epsilon^2 \Theta, \quad (17)$$

instead of (16) we get the standard LLE describing a vicinity of a single cavity resonance

$$\partial_{t_2} u = -ku - i\Theta u + i\chi u |u|^2 + ib\partial_{t_0 t_0} u + r \quad (18)$$

with the periodic boundary condition $u(t_0, t_2) = u(t_0 - 1, t_2)$.

Note finally, that in the conservative limit the LLE transforms into the nonlinear Schrödinger equation (NLSE), see also Ref. [28]. However, the existence of stable soliton solutions is hardly possible in the NDDE model near this limit. Since unlike the standard NLSE the NDDE contains the dispersion of all the orders, the next dominating order after the second one will be the third order dispersion. However, it is well known that the solitons of the NLSE are destroyed by the Cherenkov radiation [19, 1] in the presence of an arbitrary small third order dispersion term [37, 7, 9].

5 Linear stability analysis in the small amplitude conservative limit

Let us consider the linear equation

$$\begin{aligned} & A + a\partial_t A + \frac{a^2 - ib}{2}\partial_{tt} A \\ & = \left(A_\tau - a\partial_t A_\tau + \frac{a^2 + ib}{2}\partial_{tt} A_\tau \right) e^{i\theta}, \end{aligned} \quad (19)$$

obtained by the linearization of the NDDE models with $\kappa = 1$ and $\eta = 0$ at the trivial solution $A = 0$. Substituting $A(t) = A_0 e^{\lambda t}$ into (19) we get the characteristic equation

$$1 + a\lambda + \frac{a^2 - ib}{2}\lambda^2 = \left(1 - a\lambda + \frac{a + ib}{2}\lambda^2 \right) e^{-\lambda\tau}. \quad (20)$$

In the large delay limit using the approach of Ref. [39] we substitute $e^{-\lambda\tau} \equiv Y$ into Eq. (20), solve the resulting equation with respect to Y , and set $\lambda = i\nu$. Thus, we get the following expression for the pseudo-continuous spectrum in the limit $\tau \rightarrow \infty$

$$\begin{aligned} \lambda\tau &= -\ln \left[\frac{1 + ia\nu - (a^2 - ib)\nu^2/2}{1 - ia\nu - (a^2 + ib)\nu^2/2} e^{-i\theta} \right] = \\ &= -\ln e^{i\Psi(\nu) - i\theta} = -i\Psi(\nu) + i\theta \end{aligned} \quad (21)$$

with real $\Psi(\nu)$. The fact that the pseudo-continuous spectrum of Eq. (19) is purely imaginary is obviously the consequence of the reversibility of this equation, see also Ref. [28]. However, whether this system exhibits spurious instability depends on the discrete spectrum of the characteristic equation (20). In the large delay limit discrete eigenvalues with positive real parts correspond to small $|Y| \ll 1$

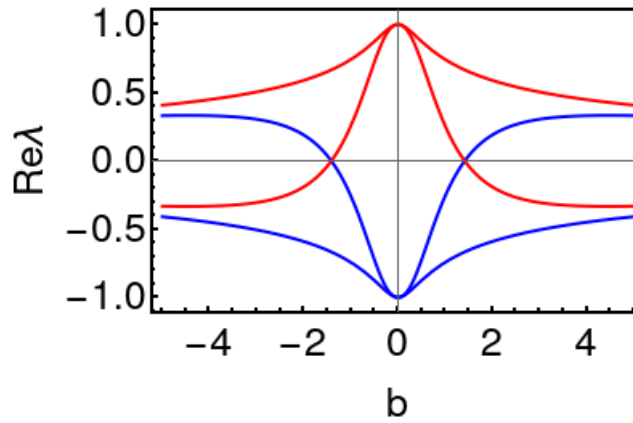


Figure 2: Real parts of the eigenvalues λ_{\pm} defined by (22) with $a = 1$ (blue) and $a = -1$ (red).

in the limit $\tau \rightarrow \infty$. Therefore, they can be obtained by equating to zero the left hand side of Eq. (20), $1 + a\lambda + (a^2 - ib)\lambda^2/2 = 0$, which gives

$$\lambda_{\pm} = \frac{-a \pm \sqrt{-a^2 + 2ib}}{a^2 - ib}. \quad (22)$$

The real parts of the eigenvalues λ_{\pm} are shown in Fig. 2 as functions of the “second order dispersion coefficient” b . It is seen that for $a < 0$ at one of the two discrete eigenvalues always has a positive real part. This means that Eq. (19) with $a < 0$ should demonstrate a spurious instability. For $a > 0$ both the eigenvalues λ_{\pm} have negative real parts if

$$|b| < \sqrt{2}a^2. \quad (23)$$

Hence, in order to avoid spurious instabilities below we choose $a > 0$ in the NDDE models and assume that the inequality (23) is satisfied. Note, that positive coefficient a can be rescaled to unity by rescaling the time variable in the model equations.

6 CW solutions

In this section we study the linear stability of the CW solutions of Eq. (1). The amplitude A of the CW solutions satisfies the equation

$$Ae^{-i\alpha|A|^2/2 - i\theta/2} = \sqrt{\kappa}Ae^{i\alpha|A|^2/2 + i\theta/2} + \eta. \quad (24)$$

Substituting into Eq. (24) $A = \sqrt{I}e^{i\varphi}$, where I and φ are the intensity and the phase of the CW solution, and separating real and imaginary parts of the resulting equation we get the following equation for the CW intensity

$$[1 + \kappa - 2\sqrt{\kappa} \cos(\theta + \alpha I)] I = \eta^2, \quad (25)$$

which is transformed into the corresponding relation of the LLE in the limit (14) and (17). The phase of the CW solution is given by

$$\tan \varphi = \frac{\sin\left(\frac{\alpha I}{2}\right) + \sqrt{\kappa} \sin\left(\theta + \frac{\alpha I}{2}\right)}{\cos\left(\frac{\alpha I}{2}\right) - \sqrt{\kappa} \cos\left(\theta + \frac{\alpha I}{2}\right)}.$$

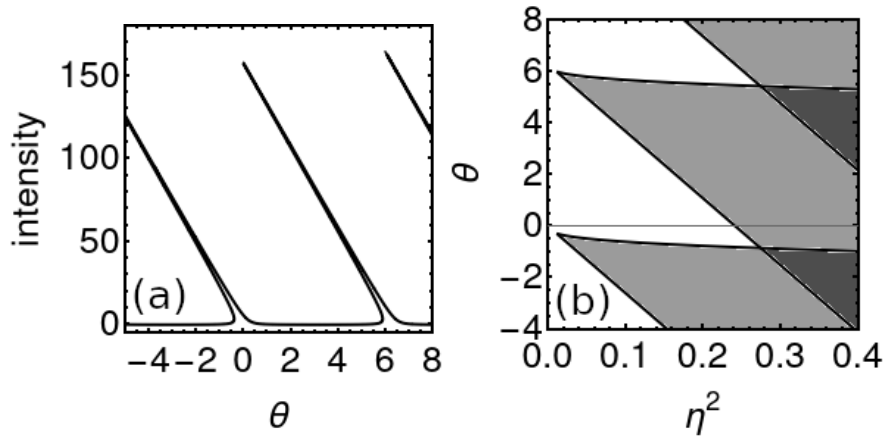


Figure 3: Intensity of CW solutions of Eq. (1) as a function of the detuning parameter θ for $\eta = 0.5$ (a). Saddle-node bifurcations of CW solutions on (η^2, θ) -plane (b). White, light gray, and dark gray areas limited by the saddle-node bifurcations indicate the existence of one, three, and five CW solutions, respectively. The parameter values $\kappa = 0.923$ and $\alpha = 0.04$ correspond to $\epsilon = 0.2$ in Eq. (14).

Nonlinear resonances of CW solutions of Eq. (1) near cusp bifurcations corresponding to different cavity modes are shown in Fig. 3(a).

The saddle-node bifurcations of the CW solutions are defined by the conditions

$$4\alpha^2\kappa I^4 - \alpha^2 I^2 [\eta^2 - (\kappa + 1) I]^2 = \eta^4,$$

$$\theta_{\pm} = \arctan \left[\frac{-(1 + \kappa) \alpha I \pm \sqrt{\kappa (4\alpha^2 I^2 + 2 - \kappa) - 1}}{1 + \kappa \pm \alpha I \sqrt{\kappa (4\alpha^2 I^2 + 2 - \kappa) - 1}} \right] - \alpha I + 2\pi n,$$

where θ_{\pm} define a pair of saddle-node bifurcations limiting the bistability domain corresponding to a single cavity resonance. Figure 3(b) illustrates the coexistence of multiple CW solutions of Eq. (1). It is seen that at sufficiently high injection rates the CW resonances start overlapping. Unlike the resonances shown in Fig. 3(b), the bistability domains of Eq. (11) with cubic nonlinearity are much more narrow and never overlap. This can be easily understood by noticing that for cubic nonlinearity Eq. (25) transforms into a cubic equation in I having not more than three solutions. Hence, the mean field model (11) does not describe well the dynamics of Eq. (1) beyond the LLE limit. Therefore, below we focus mainly on the model (1), which does not assume the mean field approximation.

To study the linear stability of the CW solution we linearize Eq. (1) around this solution, $A(t) = (\sqrt{I} + \delta A e^{\lambda t}) e^{i\varphi}$. Thus we get the following characteristic equation:

$$c_2 Y^2 + c_1 Y + c_0 = 0, \quad (26)$$

where $Y(\lambda) = \exp(-\lambda\tau)$, and the coefficients $c_{0,1,2}$ are polynomials in λ :

$$c_2 = \kappa + \frac{\kappa\lambda}{4} [(a^4 + b^2) \lambda^3 - 4a^3 \lambda^2 + 2(4a^2 - b\alpha I) \lambda - 8a],$$

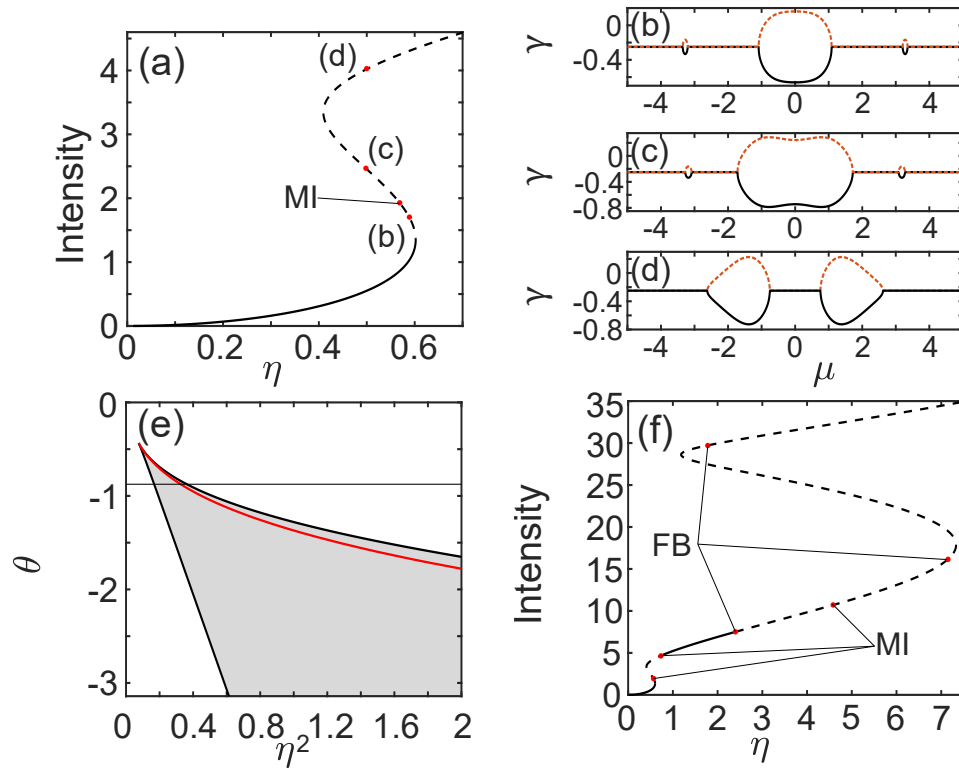


Figure 4: S-shaped dependence of the intensity I of CW solutions on the injection rate η (a). Curves of pseudocontinuous spectrum for different values of I (b) $I \approx 1.7032$, (c) $I \approx 2.4643$, (d) $I \approx 4.0221$. Saddle-node bifurcations (black curves) and modulational instability (red curve) around a single cavity resonance on the (θ, η^2) -plane (e). CW solutions from (a) in the region of larger η and I (f). Parameters are: $\epsilon = 0.5$, $\kappa = e^{-2\epsilon^2}$, $\alpha = 1\epsilon^2$, $\theta = -3.5\epsilon^2$, $a = 1\epsilon$, $b = -1\epsilon^2$. Unstable solutions are shown by dashed line. MI (FB) indicates the modulational (flip) bifurcation points.

$$c_1 = \frac{\sqrt{\kappa}}{2} \left\{ [(b^2 - a^4) \lambda^4 - 2b\alpha I \lambda^2 - 4] \cos(\alpha I + \theta) + 2(2 + a^2 \lambda^2)(\alpha I - b\lambda^2) \sin(\alpha I + \theta) \right\} \quad (27)$$

$$c_0 = \frac{1}{4} \left[(a^4 + b^2) \lambda^4 + 4a^3 \lambda^3 + 2(4a^2 - b\alpha I) \lambda^2 + 8a\lambda + 4 \right].$$

In the limit of large delay time $\tau \rightarrow \infty$ the eigenvalues of the pseudo-continuous spectrum (PCS) can be represented as $\lambda \approx i\mu + \gamma/\tau$ with real μ and γ [39]. The pseudo-continuous spectrum is given by the two solution branches of the quadratic equation (26):

$$\gamma(\mu) = -\text{Re} \{ \ln [Y(i\mu)] \}. \quad (28)$$

Stable CW solutions are characterized by $\gamma(\mu) < 0$ and, in particular, $\gamma(0) < 0$. At the saddle-node (flip) bifurcation point we have $\gamma(0) = 0$ and $Y(0) = 1$ ($\gamma(0) = 0$ and $Y(0) = -1$), while modulational instability takes place when one or both branches of pseudocontinuous spectrum are tangent to the imaginary axis at $\mu = \pm\mu_m$ with $|\mu_m| > 0$.

S-shaped CW curve of Eq. (1) is shown in Fig. 4(a). It is seen that modulational instability takes place on the unstable middle part of the CW curve and destabilizes its upper part. Figures 4(c)-(d) present the real parts of the pseudo-continuous eigenvalues $\gamma(\mu)$ calculated at the points indicated in 4(a). Figure 4(e) illustrates the location of the modulational instability curve between two saddle-node bifurcations around a single cavity resonance in (η^2, θ) -plane. Finally, Fig. 4(f) illustrates a growing

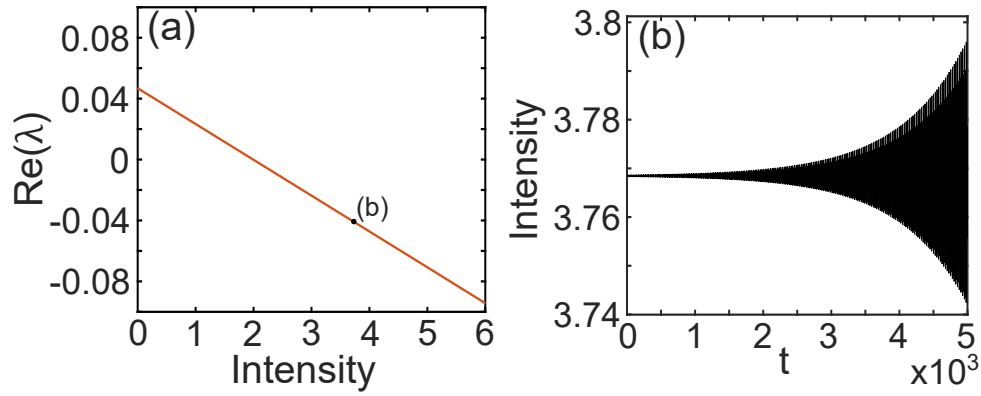


Figure 5: Largest real part of the discrete eigenvalues of the CW solution with $b = (\sqrt{2} + 0.01)a^2$ as a function of the CW intensity I (a). $a = 0.1$. Evolution of the (modulationally unstable) state from the upper bifurcation branch with $\eta = 0.02$ (b). The solution diverges with time. Other parameters are the same as in Fig. 4 except $\epsilon = 0.1$.

multiplicity of the solutions of Eq. (25) due to the overlap of resonances with increasing the injection rate.

It is important also to check the discrete spectrum of nonlinear CW solutions. The discrete spectrum is defined by the instantaneous part of the model equation and can be obtained by solving the equation $c_0 = 0$ with respect to λ , where c_0 is defined by Eqs. (26) and (27). It is seen from Fig. 5 corresponding to $b = (\sqrt{2} + 0.01)a^2$ that when b exceeds slightly the critical value defined by (23) the lower part of the CW branch can become unstable with respect to the discrete spectrum, see Fig. 5(a). The increase of the CW intensity I has a stabilizing effect on the discrete spectrum. However, as it is seen from Fig. 5(b) the solution of Eq. (1) starting from the upper CW state becomes unbounded in the limit $t \rightarrow \infty$. This behavior might be attributed to a spurious instability.

7 Cavity solitons

In this section we investigate numerically TCS solutions of the NDDE models using the RADAR5 code written in FORTRAN [11]. We start with the delay time $\tau = 25$ and the parameter values close to the LLE limit defined by Eqs. (14) and (17), $\kappa = e^{-2\epsilon^2}$, $\alpha = \epsilon^2$, $a = \epsilon$, $b = \epsilon^2$, $\theta = -3.5\epsilon^2$, $\eta = 1.855\epsilon^2$ with $\epsilon = 0.02$. The calculated TCS solution of Eq. (1) is shown in Fig. 6(a) by black line. This soliton is very close to the TCS of the model (5) shown by green line. Dissipative soliton of the LLE (18) is indicated by red dashed line in the same figure for the LLE parameter values obtained using the relations (14) and (17), $k = 1$, $\Theta = -3.5$, $\chi = 1$, $b = 1$, $r = 1.855$ in Eq. (18). With increasing ϵ the soliton profile gets more asymmetric, see Figs. 6(c) and (d) obtained with $\epsilon = 0.1$. As it is seen in Fig. (d), the soliton tails exhibit slowly decaying oscillations, which can be attributed to the so-called Cherenkov radiation induced by high order dispersion [18, 1]. The Cherenkov radiation amplitude increases with ϵ , see Fig. 6(b) obtained with $\epsilon = 0.34$ and eventually destroys the TCS.

The dependence of the TCS peak power on the parameter ϵ calculated using the models (1) (black line) and (5) (blue line) with exponential nonlinearity, and the model (11) (red line) with cubic nonlinearity is shown in Fig. 7. It is seen that while sufficiently close to the LLE limit, $\epsilon \rightarrow 0$, this dependence looks rather smooth, it becomes fast oscillating with the increase of ϵ . Such oscillatory behavior can be explained by the interaction of a TCS with its own tails leading either to constructive or destructive

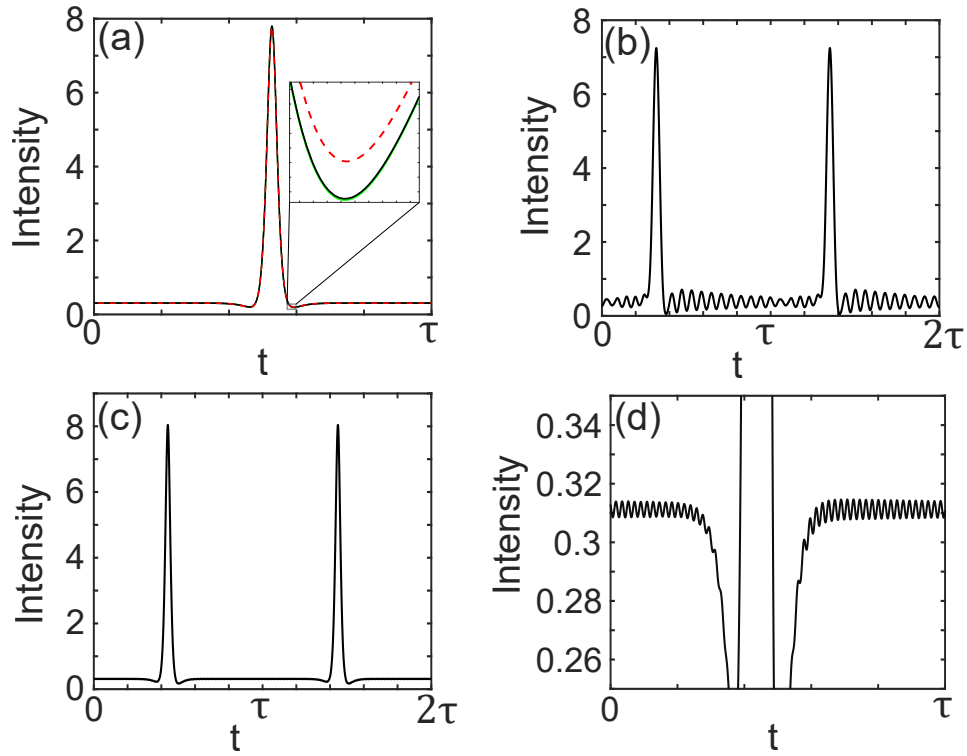


Figure 6: TCS profiles calculated using the model equations (1) (black line) with $\epsilon = 0.02$ (a), $\epsilon = 0.34$ (b), $\epsilon = 0.1$ (c) and (d). Other parameters are given in the text. One can see from panel (d) that already for $\epsilon = 0.1$ the TCS tails exhibit a Cherenkov radiation, which is more pronounced at the trailing tail. In panel (a) the TCS of Eq. (5) is shown by green line and the soliton of the LLE (18) - by red dashed line. Parameters are: $\kappa = e^{-2\epsilon^2}$, $\alpha = \epsilon^2$, $a = \epsilon$, $b = \epsilon^2$, $\theta = -3.5\epsilon^2$, $\eta = 1.855\epsilon^2$.

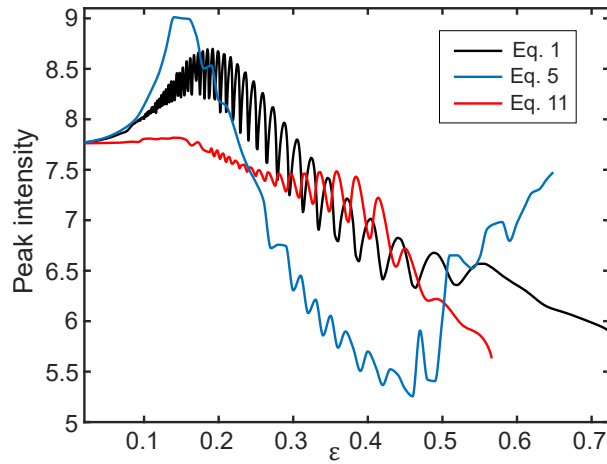


Figure 7: TCS peak power as a function of the parameter ϵ calculated using Eq. (1) (black), Eq. (5) (blue), and Eq. (11) (red) with $\eta = 1.855\epsilon^2$ and $\tau = 25$. Other parameters are the same as in Fig.6.

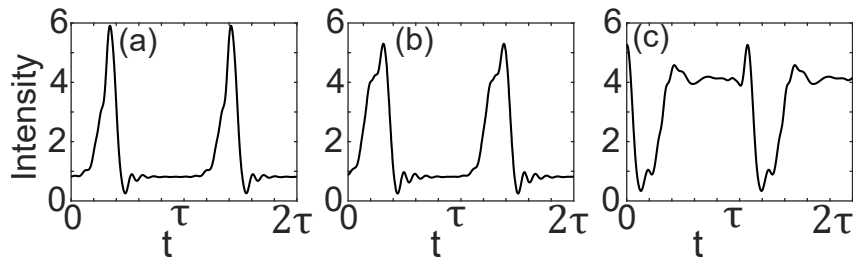


Figure 8: Different types of localizes solutions of the NDDE model (1) calculated for $\epsilon = 0.722$. The TCS shown in panel (a) corresponds to the black curve shown in Fig.7. Other parameters are the same as in Fig.7.

interference due to the presence of Cherenkov radiation. Furthermore, it is seen that the oscillation frequency increases with the decrease of ϵ , which is in agreement with the fact that the frequency of the Cherenkov radiation tends to infinity when the third and/or fourth order dispersion coefficients tend to zero, see e. g. [35, 36]. Note that the more exact model (5) demonstrates weaker dependence of the TCS peak power on the Cherenkov radiation than Eq. (1). Therefore, Eq. (5) may be more suitable for the description of the system dynamics far away from the LLE limit.

At relatively high values of ϵ different types of TCS can appear, as it is shown in Fig. 8. Their stability ranges in the parameter space are relatively small, but with $\epsilon = 0.722$ can coexist for the same set of parameters.

It is known that the soliton of the LLE can undergo an oscillatory instability with the increase of the injection rate. The NDDE model (1) also shows a similar behavior. Figure 9 illustrates the appearance of undamped oscillations of the soliton peak power for fixed relatively small $\epsilon = 0.05$. At higher values of ϵ there are different types of oscillating TCSs.

8 Conclusion

To conclude, we have developed a second order NDDE model of a ring dispersive Kerr cavity with a coherent optical injection. Similarly to the first order NDDE model discussed in [28] in the non-

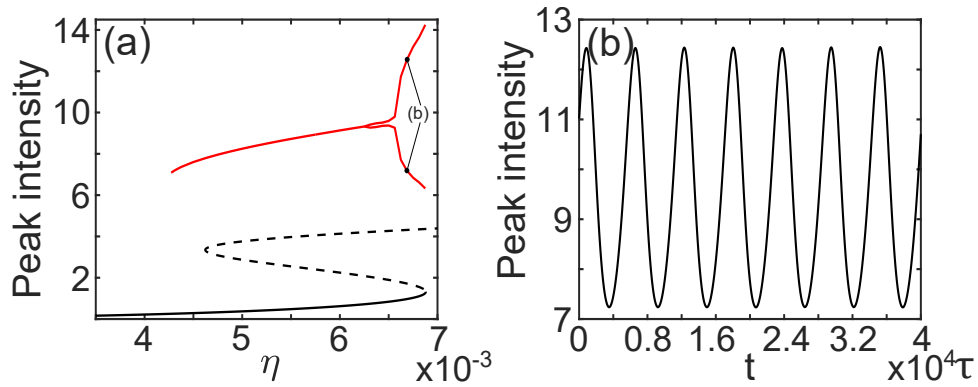


Figure 9: TCS peak power (red curve) and intensity of CW solution (black curve) as functions of the injection rate η (a). The TCS starts to oscillate above the Andronov-Hopf bifurcation threshold at $\eta \approx 6.25 \times 10^{-3}$. Red lines show maximal and minimal peak power within the oscillation period. Time-trace of the TCS peak power calculated for $\eta = 6.7 \times 10^{-3}$ (b). $\epsilon = 0.05$. Other parameters are the same as in Fig.7

dissipative limit this model is reversible and has a conserved quantity. In a certain parameter range and under the mean field and large delay approximations the NDDE model can be reduced to the famous LLE model. However, unlike the LLE and similarly to the Ikeda map [12] and generalized LLE [20] Kerr cavity models, the NDDE model is able to describe the overlap of the resonances associated with different cavity modes. We have shown that TCSs can exist in the NDDE model not only close to the LLE limit, but also beyond this limit. In the latter case they are strongly affected by the Cherenkov radiation, which is induced by high order dispersion and eventually destroys the TCS. An important advantage of the NDDE model is that it can be analyzed numerically using standard codes, such as RADAR5 [11] and DDE-biftool [8]. Furthermore, after appropriate modifications this model can be applied to study the dynamics of soliton mode-locked lasers and other laser systems where the chromatic dispersion of the intracavity material dominates over the spectral filtering in the mechanism of the short pulse formation. The NDDE model might be also useful for the consideration of the coupled-cavity systems, such as an optical microcavity pumped by a semiconductor mode-locked laser modeled by the DDE mode-locking model [33, 34, 32]. This model can be easily extended by including higher order dispersion terms into it.

References

- [1] N. Akhmediev and M. Karlsson. Cherenkov radiation emitted by solitons in optical fibers. *Phys. Rev. A*, 51(3):2602–2607, 1995.
- [2] Y. K. Chembo and C. R. Menyuk. Spatiotemporal lugiato-lefever formalism for kerr-comb generation in whispering-gallery-mode resonators. *Phys. Rev. A*, 87:053852, 2013.
- [3] S. Coen and M. Haelterman. Modulational instability induced by cavity boundary conditions in a normally dispersive optical fiber. *Physical review letters*, 79(21):4139, 1997.
- [4] S. Coen, H. G. Randle, T. Sylvestre, and M. Erkintalo. Modeling of octave-spanning kerr frequency combs using a generalized mean-field lugiato-lefever model. *Optics letters*, 38(1):37–39, 2013.

- [5] S. T. Cundiff and J. Ye. Colloquium: Femtosecond optical frequency combs. *Reviews of Modern Physics*, 75(1):325, 2003.
- [6] P. Del'Haye, A. Schliesser, O. Arcizet, T. Wilken, R. Holzwarth, and T. J. Kippenberg. Optical frequency comb generation from a monolithic microresonator. *Nature*, 450(7173):1214–1217, 2007.
- [7] J. Elgin. Soliton propagation in an optical fiber with third-order dispersion. *Optics letters*, 17(20):1409–1410, 1992.
- [8] K. Engelborghs, T. Luzyanina, and G. Samaey. DDE-BIFTOOL v.2.00: A MATLAB package for bifurcation analysis of delay differential equations. Technical Report TW-330, Department of Computer Science, K.U.Leuven, Leuven, Belgium, 2001.
- [9] J. P. Gordon. Dispersive perturbations of solitons of the nonlinear schrödinger equation. *JOSA B*, 9(1):91–97, 1992.
- [10] P. Grelu and N. Akhmediev. Dissipative solitons for mode-locked lasers. *Nature photonics*, 6(2):84–92, 2012.
- [11] N. Guglielmi and E. Hairer. Implementing radau iia methods for stiff delay differential equations. *Computing*, 67(1):1–12, 2001.
- [12] M. Haelterman, S. Trillo, and S. Wabnitz. Dissipative modulation instability in a nonlinear dispersive ring cavity. *Optics communications*, 91(5-6):401–407, 1992.
- [13] T. Hansson and S. Wabnitz. Frequency comb generation beyond the lugiato–lefever equation: multi-stability and super cavity solitons. *JOSA B*, 32(7):1259–1266, 2015.
- [14] T. Herr, V. Brasch, J. D. Jost, C. Y. Wang, N. M. Kondratiev, M. L. Gorodetsky, and T. J. Kippenberg. Temporal solitons in optical microresonators. *Nature Photonics*, 8:145–152, 2014.
- [15] M. Heuck, S. Blaaberg, and J. Mørk. Theory of passively mode-locked photonic crystal semiconductor lasers. *Optics express*, 18(17):18003–18014, 2010.
- [16] K. Ikeda. Multiple-valued stationary state and its instability of the transmitted light by a ring cavity system. *Optics communications*, 30(2):257–261, 1979.
- [17] D. J. Jones, S. A. Diddams, J. K. Ranka, A. Stentz, R. S. Windeler, J. L. Hall, and S. T. Cundiff. Carrier-envelope phase control of femtosecond mode-locked lasers and direct optical frequency synthesis. *Science*, 288(5466):635–639, 2000.
- [18] V. Karpman. Radiation by solitons due to higher-order dispersion. *Physical Review E*, 47(3):2073, 1993.
- [19] V. I. Karpman. Radiation by solitons due to higher-order dispersion. *Phys. Rev. E*, 47:2073–2082, 1993.
- [20] Y. Kartashov, O. Alexander, and D. Skryabin. Multistability and coexisting soliton combs in ring resonators: the Lugiato-Lefever approach. *Optics Express*, 25(10):11550–11555, 2017.
- [21] T. Kolokolnikov, M. Nizette, T. Erneux, N. Joly, and S. Bielawski. The q-switching instability in passively mode-locked lasers. *Physica D: Nonlinear Phenomena*, 219(1):13–21, 2006.

- [22] F. Leo, S. Coen, P. Kockaert, S.-P. Gorza, P. Emplit, and M. Haelterman. Temporal cavity solitons in one-dimensional kerr media as bits in an all-optical buffer. *Nature Photonics*, 4:471–476, 2010.
- [23] L. A. Lugiato and R. Lefever. Spatial dissipative structures in passive optical systems. *Physical review letters*, 58(21):2209, 1987.
- [24] D. Mc Laughlin, J. V. Moloney, and A. C. Newell. Solitary waves as fixed points of infinite-dimensional maps in an optical bistable ring cavity. *Physical review letters*, 51(2):75, 1983.
- [25] N. Picqué and T. W. Hänsch. Frequency comb spectroscopy. *Nature Photonics*, 13(3):146–157, 2019.
- [26] A. Pimenov and A. G. Vladimirov. Temporal solitons in an optically injected kerr cavity with two spectral filters. *Optics*, 3(4):364–383, 2022.
- [27] J. Schröder, A. Fülöp, M. Mazur, L. Lundberg, Ó. B. Helgason, M. Karlsson, P. A. Andrekson, et al. Laser frequency combs for coherent optical communications. *Journal of Lightwave Technology*, 37(7):1663–1670, 2019.
- [28] T. Seidel, S. Gurevich, and J. Javaloyes. Conservative solitons and reversibility in time delayed systems. *Physical Review Letters*, 128(8):083901, 2022.
- [29] M.-G. Suh, X. Yi, Y.-H. Lai, S. Leifer, I. S. Grudinin, G. Vasisht, E. C. Martin, M. P. Fitzgerald, G. Doppmann, J. Wang, et al. Searching for exoplanets using a microresonator astrocomb. *Nature photonics*, 13(1):25–30, 2019.
- [30] P. Trocha, M. Karpov, D. Ganin, M. H. Pfeiffer, A. Kordts, S. Wolf, J. Krockenberger, P. Marin-Palomo, C. Weimann, S. Randel, et al. Ultrafast optical ranging using microresonator soliton frequency combs. *Science*, 359(6378):887–891, 2018.
- [31] E. A. Viktorov, P. Mandel, A. G. Vladimirov, and U. Bandelow. Model for mode locking in quantum dot lasers. *Applied physics letters*, 88(20):201102, 2006.
- [32] A. G. Vladimirov and D. Turaev. New model for mode-locking in semiconductor lasers. *Radiophys. & Quant. Electron.*, 47(10-11):857–865, 2004.
- [33] A. G. Vladimirov and D. Turaev. Model for passive mode-locking in semiconductor lasers. *Phys. Rev. A*, 72:033808 (13 pages), 2005.
- [34] A. G. Vladimirov, D. Turaev, and G. Kozyreff. Delay differential equations for mode-locked semiconductor lasers. *Opt. Lett.*, 29:1221–1223, 2004.
- [35] A. G. Vladimirov, S. V. Gurevich, and M. Tlidi. Effect of cherenkov radiation on localized-state interaction. *Physical Review A*, 97(1):013816, 2018.
- [36] A. G. Vladimirov, M. Tlidi, and M. Taki. Dissipative soliton interaction in kerr resonators with high-order dispersion. *Physical Review A*, 103(6):063505, 2021.
- [37] P. K. A. Wai, H. H. Chen, and Y. C. Lee. Radiations by Bolitons at the zero group-dispersion of single-mode optical fibers. *Phys. Rev. A*, 41:426–439, 1990.
- [38] X. Xue and A. M. Weiner. Microwave photonics connected with microresonator frequency combs. *Frontiers of Optoelectronics*, 9(2):238–248, 2016.

- [39] S. Yanchuk and M. Wolfrum. A multiple time scale approach to the stability of external cavity modes in the Lang-Kobayashi system using the limit of large delay. *SIAM J. Appl. Dyn. Syst.*, 9: 519–535, 2010. doi: 10.1137/090751335.